

Stochastic model of endosomal escape of Influenza virus

Thibault Lagache · Christian Sieben ·
Tim Meyer · Andreas Herrmann ·
David Holcman

Received: XX/ Accepted: XX

Abstract Keywords Mathematical Modeling · Markov Jump Process ·
WKB approximation · Endosomal Acidification · Influenza

PACS 87.10.Mn · 87.16.Wd · 87.16.ad · 87.16.af

Mathematics Subject Classification (2000) 92-08 · 60J75 · 35Q84 ·
81S22 · 34E20

T. Lagache
Applied Mathematics and Computational Biology, IBENS, Ecole Normale Supérieure, 46
rue d'Ulm 75005 PARIS, France
E-mail: thibault.lagache@pasteur.fr
Present address: BioImage Analysis Unit, CNRS UMR 3671, Institut Pasteur, France.

C. Sieben
Department of Biology, Molecular Biophysics, IRI Life Sciences, Humboldt-Universität zu
Berlin, Germany

T. Meyer
Institute of Chemistry and Biochemistry, Free University Berlin, Germany

A. Herrmann
Department of Biology, Molecular Biophysics, IRI Life Sciences, Humboldt-Universität zu
Berlin, Germany

D. Holcman
Applied Mathematics and Computational Biology, IBENS, Ecole Normale Supérieure, 46
rue d'Ulm 75005 PARIS, France and Newton Institute, DAMTP Cambridge CB3 0DS and
Mathematical Institute, University of Oxford, Andrew Wiles Building, Woodstock Rd, Ox-
ford OX2 6GG, United Kingdom
E-mail: david.holcman@ens.fr

1 Abstract

Influenza viruses enter a cell via endocytosis after binding to the surface. During the endosomal journey, acidification triggers a conformational change of the virus spike protein hemagglutinin (HA) that results in escape of the viral genome from the endosome to the cytoplasm. A quantitative understanding of the processes involved in HA mediated fusion with the endosome is still missing. We develop here a stochastic model to estimate the change of conformation of HAs inside the endosome nanodomain. Using a Markov-jump process to model the arrival of protons to HA binding sites, we compute the kinetics of their accumulation and the mean first time for HAs to be activated. This analysis reveals that HA proton binding sites possess a high chemical barrier, ensuring a stability of the spike protein at sub-acidic pH. Finally, we predict that activating more than 3 adjacent HAs is necessary to prevent a premature fusion.

2 Introduction

The first step of infection by influenza starts when viral particles enter the cell by a process called endocytosis at the host cell surface, where they are captured in spherical endosome. The second step is the transport of the virus, trapped inside the endosome. During the third and critical step, the viral genome, encoding ribonucleoproteins (vRNPs) has to escape from the endosomal compartment, so that later on, it can translocate into the nucleus [23] (Figure 1-A). Fusion between the endosome and influenza virus is mediated by a low-pH conformational change of the viral envelope glycoprotein hemagglutinin (HA) (figure 1-A). The goal of this article is to present a new model based on endosome acidification and conformational change of the HA to predict the exact timing for initiating fusion between the virus and the endosome membrane, and thus to release the viral genome.

The model accounts for important detailed properties of the glycoprotein HA composed by two linked subunits HA1 and HA2, the latter anchoring HA to the viral envelope. Indeed, at neutral pH, HA is not active (in a non-fusogenic state), but as the pH decreases due to proton entry into the endosome, a partial dissociation of the HA1 subunit results in a spring-loaded conformational change of HA2 into an active (fusogenic) state [9]. Consequently, the residence time of influenza virus genome within the endosome before fusion depends on the kinetics of endosome acidification. Yet, the absence of direct in vivo measurements of these parameters makes the endosomal step of virus infection difficult to analyze. To estimate the pH-driven fusion of influenza viruses in an endosome, we develop a model that accounts for the main kinetics parameters of the fusion process.

We start by developing a kinetics model for endosome acidification, that we calibrate using experimental data. The model depends on the following parameters: buffering capacity of the endosomal lumen, membrane leakage and proton pumping rate, all together controlling the number of free protons inside the endosome. Because the proton binding event to HA is discrete, we model it here using a classical Markov jump process [27]. Using an asymptotic expansion of the solution for the mean arrival time equation for the number of protons to a certain threshold, we obtain an analytical expression for the kinetics of HA conformational change at fix pH values. The model is then calibrated using the kinetics of the HA conformational change [16]. Finally, by combining the two models for kinetics of endosomal acidification and HA conformational change, we can estimate the number of activated HAs inside an endosome. We predict that at least three adjacent activated HAs are necessary to trigger membrane fusion [4, 11], a cooperativity process that should prevent premature fusion. We confirm some of the predictions using co-labeling viruses and endosomal markers experimental data, showing that intracellular fusion of viruses mainly occur in maturing endosomes.

3 Kinetics model of endosomal acidification

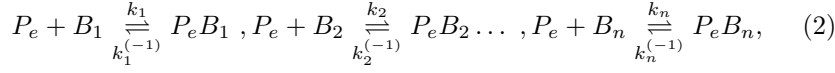
The model of endosomal acidification follows the free number of protons $P_e(t)$ at time t in the endosomal compartment. The protons enter with an entry rate $\lambda(t)S$ through the V-ATPase proton pumps (S is the endosomal surface and the rate $\lambda(t)$ is associated with to the proton pumps activity) and can escape with a leaking rate $L_{ext}(t)$, but can also bind to endosomal buffers. The proton pump rate $\lambda(t)$ is mainly determined by the membrane potential $\Psi(t)$ (Figure 11 [7]), which in turn depends on the endosomal concentrations of several cations ($H^+, K^+, Na^+ \dots$) and ($Cl^- \dots$). The ionic concentration inside endosome is tightly regulated by channels, exchangers and leak and in particular, by raising the interior-positive membrane potential, Na-K ATPase exchangers have been proposed to limit the acidification of early compared to late endosomes [5].

3.1 Mass action law for free protons

To derive the time-dependent equations for the free protons, we use the balance of fluxes. The fast equilibrium between fluxes determines the effective number of protons $P_e(t)dt$ entering the endosome which follows the first order kinetics

$$\frac{dP_e}{dt} = (\lambda(t)S - L_{ext}(t)). \quad (1)$$

Protons are rapidly bound to endosomal buffers. We model the buffer activity using an ensemble of chemical reactions $(P_e B_i / B_i)_{1 \leq i \leq n}$ [6]:



where $(k_i, k_i^{(-1)})_{1 \leq i \leq n}$ are the rate constants $(P_e B_i / B_i)_{1 \leq i \leq n}$. Thus the kinetics equations for the number of free protons $P_e(t)$ inside an endosome is

$$\begin{aligned} \frac{dP_e(t)}{dt} &= \Delta P_e(t) + \sum_{i=1}^n \left(k_i^{(-1)} P_e B_i(t) - \frac{k_i}{N_A V_e} P_e(t) B_i(t) \right) \\ &= (\lambda(t)S - L_{ext}(t)) + \sum_{i=1}^n \left(k_i^{(-1)} P_e B_i(t) - \frac{k_i}{N_A V_e} P_e(t) B_i(t) \right), \end{aligned}$$

where $P_e B_i(t)$ and $B_i(t)$ are the number of weak acids and bases inside the endosome at time t . We assume that the membrane potential $\Psi(t)$ reaches rapidly its steady state value $\Psi(\infty)$ compared to the acidification kinetics [7], we thus approximate the pumping rate $\lambda(t)S$ as

$$\lambda(t)S \approx \lambda S. \quad (3)$$

where the parameter λ is related to the membrane potential $\Psi(\infty)$. In addition, the protons leak $L_{ext}(t)$ is proportional to the endosomal concentration and the endosomal surface [6]

$$L_{ext}(t) = LS \frac{P_e(t)}{N_A V_e}, \quad (4)$$

where L is a permeability constant, N_A is the Avogadro constant and V_e is the volume of the endosome. Consequently, using approximations 3-4 in equation 3, we obtain the general dynamics of free protons:

$$\frac{dP_e(t)}{dt} = \left(\lambda - L \frac{P_e(t)}{N_A V_e} \right) S + \sum_{i=1}^n \left(k_i^{(-1)} P_e B_i(t) - \frac{k_i}{N_A V_e} P_e(t) B_i(t) \right).$$

3.2 Dynamics of the pH and the steady state limit

When the protons enter the endosome, they equilibrate with buffers, a process much faster compared to acidification: after a fraction of $\Delta P_e(t)$ protons have entered the endosome, they instantaneously bind to bases, leading to a jump $-\Delta B_i(t)$ on each base

$$\Delta P_e(t) \approx - \sum_{i=1}^n \Delta B_i(t). \quad (5)$$

To estimate the associated pH change $d\text{pH}$ with the entry $\Delta P_e(t)$ of protons and the infinitesimal changes $-dB_i(t)$ of the number of bases, we use equation 2) at equilibrium and time t :

$$k_i^{(-1)} P_e B_i(t) = k_i \frac{P_e(t) B_i(t)}{N_A V_e}, \text{ for all } 1 \leq i \leq n. \quad (6)$$

Thus,

$$\frac{P_e(t)}{N_A V_e} = K_i \frac{C_i - B_i(t)}{B_i(t)}, \text{ for all } 1 \leq i \leq n, \quad (7)$$

where $K_i = \frac{k_i^{(-1)}}{k_i}$ and $C_i = P_e B_i(0) + B_i(0)$ are constant. Consequently,

$$\text{pH}(t) = pK_i + \frac{1}{\log(10)} \log \left(\frac{B_i(t)}{(C_i - B_i(t))} \right) \quad (8)$$

where $pK_i = -\log(K_i)/\log(10)$. By differentiating equation 8 with respect to B_i , the infinitesimal variation dB_i of base i is related to $d\text{pH}$ of the endosomal pH by

$$d\text{pH} = \left(\frac{1}{\log(10)} \frac{C_i}{B_i(t) (C_i - B_i(t))} \right) dB_i. \quad (9)$$

Using equation 7, we get for equation 9

$$d\text{pH} = \left(\frac{1}{\log(10)} \frac{(N_A V_e K_i + P_e(t))^2}{P_e(t) C_i N_A V_e} \right) dB_i, \quad (10)$$

leading to

$$dB_i = N_A V_e \beta_i (P_e(t)) d\text{pH}, \quad (11)$$

where

$$\beta_i (P_e(t)) = \log(10) C_i \frac{P_e(t) K_i}{(P_e(t) + K_i N_A V_e)^2} \quad (12)$$

is the buffering capacity of the weak acid-base $(P_e B_i, B_i)$. Finally, using equations 5 and 11 we find that the variation $\Delta P_e(t)$ of protons is related to an infinitesimal change ΔpH of the endosomal pH through

$$\Delta P_e(t) = - \sum_{i=1}^n \Delta B_i = -N_A V_e \left(\sum_{i=1}^n \beta_i (P_e(t)) \right) \Delta \text{pH} = -N_A V_e \beta_e^0 (P_e(t)) \Delta \text{pH}, \quad (13)$$

where $\beta_e^0 (P_e(t)) = \sum_{i=1}^n \beta_i (P_e(t))$ is the total buffering capacity of the endosome, which is approximately constant $\beta_e^0 (P_e(t)) \approx \beta_e^0 = 40 \text{ mM/pH}$ [32].

Finally, using the proton extrusion and pumping rates (equation 3 and 4), we obtain the kinetics equation

$$\left(\lambda - L \frac{P_e(t)}{N_A V_e} \right) S dt = -N_A V_e \beta_e d\text{pH}. \quad (14)$$

With

$$\frac{d\text{pH}(t)}{dt} = -\frac{1}{\log(10)P_e(t)} \frac{dP_e(t)}{dt}, \quad (15)$$

we obtain that the kinetics equation for free protons accumulation in an endosome is

$$\frac{dP_e(t)}{dt} = \left(\lambda - L \frac{P_e(t)}{N_A V_e} \right) \frac{S \log(10) P_e(t)}{N_A V_e \beta_e}. \quad (16)$$

When the proton leakage is counterbalanced by the pumps, after a time long enough, the pH reaches an asymptotic value pH_∞ , where the endosome cannot be further acidified given by

$$P_e(\infty) = N_A V_e 10^{-\text{pH}_\infty}, \quad (17)$$

Consequently, the rate λ is linked to pH_∞ by

$$\lambda = L 10^{-\text{pH}_\infty}, \quad (18)$$

and equation 16 can be rewritten as

$$\frac{dP_e(t)}{dt} = \left(10^{-\text{pH}_\infty} - \frac{P_e(t)}{N_A V_e} \right) \frac{LS \log(10) P_e(t)}{N_A V_e \beta_e}. \quad (19)$$

To conclude, we obtain here a kinetics equation for the endosome acidification as a function of endosome parameters and permeability. However, equation 19 is not sufficient to account for the different stages of the endosomal maturation. Indeed, the final pH_∞ [23] and the permeability L were reported to decrease with the endosomal maturation [5] and are thus time dependent.

3.3 Modeling pH change and acidification of an endosome

We now relate the acidification dynamics to the change of two proteins that can be followed experimentally. Indeed, the transition from a first stage endosome called early endosome (EE) to a second stage endosome called late endosome (LE) is quantified by a gradual exchange of a protein called Rab5 by another one associated to the late phase called protein Rab7 [25]. Kinetics of Rab exchange have been experimentally measured and we approximate here the kinetics of the ratio Rab5/Rab7 obtained from data (Figure 4-C [25]) by a sigmoidal function

$$\frac{\text{Rab7}(t)}{\text{Rab5}(t) + \text{Rab7}(t)} = \frac{1}{1 + e^{-(t-t_{1/2})/\tau_c}}, \quad (20)$$

where $t_{1/2}$ is the half-maturation time and τ_c is the time scale of Rab conversion. We then approximate the transition rate from early to late endosome

with the Rab conversion rate and we consider that the steady-state $\text{pH}_\infty(t)$ relative to the amount of Rab7, that gradually replaces Rab5 during endosomal maturation is given by

$$\text{pH}_\infty(t) = \text{pH}_\infty^{\text{early}} + \left(\text{pH}_\infty^{\text{late}} - \text{pH}_\infty^{\text{early}} \right) \frac{\text{Rab7}(t)}{\text{Rab5}(t) + \text{Rab7}(t)}. \quad (21)$$

Similarly, the permeability constant follows the equation

$$L(t) = L^{\text{early}} + \left(L^{\text{late}} - L^{\text{early}} \right) \frac{\text{Rab7}(t)}{\text{Rab5}(t) + \text{Rab7}(t)}. \quad (22)$$

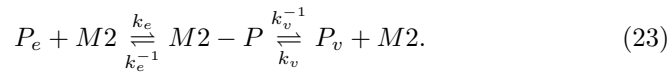
3.4 Calibrating the acidification model by live cell imaging

We shall now calibrate the acidification equation to experimental parameters. First, by fitting equation 20 to the experimental data (Figure4-C of [25]) where the lag time between initiation and termination of the Rab5/Rab7 replacement is estimated to ≈ 10 min., leading to a time constant for $\tau_c \approx 100$ s.

We use data from endosomal acidification in MDCK cells where the pH inside endosomes decreases very quickly within the first 10-15 min (Figure 1-B) to reach a steady state pH around 5.5 after 20 min, in agreement with previous studies [35]. The steady state pH is $\text{pH}_\infty^{\text{early}} = 6.0$ and $\text{pH}_\infty^{\text{late}} = 5.5$ for early and late endosomes, respectively [2], thus we calibrated the permeability constant L and Rab conversion kinetics by solving numerically equation 19 and fitting the experimental acidification curve (Figure 1-C). We found that the permeabilities of early and late endosomes are $L^{\text{early}} \approx 3.5 \cdot 10^{-3} N_A \text{cm s}^{-1}$ and $L^{\text{late}} \approx 0.1 L^{\text{early}} = 3.5 \cdot 10^{-4} N_A \text{cm s}^{-1}$, respectively and the half-maturation time is $t_{1/2} = 10$ min.

3.5 Accounting for proton influx inside viral core and buffering

The last step of the kinetics model of protons include the binding and unbinding with various viral components providing buffer capacity. Indeed, the buffering capacity of the viral proteins and the influx of protons through M2-channels inside the viral core (Figure1-A), the presence of viruses inside endosomes changes the overall buffering capacity of the endosome itself and can perturb the overall acidification kinetics. To compute the influx in each virus through M2 channels, we use first order transport kinetics [20], summarized by the chemical reaction



When a proton P_e binds a free $M2$ protein channel with a binding k_e and unbinding k_e^{-1} rates, it is transported inside the virus core with an inward rate k_v^{-1} , while the forward rate is k_v . Thus the inward flux in a single virus can be computed from equation 23 [20]

$$j_{M2}(P_e, P_v) = n_{M2} \frac{k_e^{-1} - \frac{k_e P_e \alpha(P_e, P_v)}{N_A V_e}}{1 + \alpha(P_e, P_v)}, \quad (24)$$

where n_{M2} is the number of M2 channels per viral particle, P_v is the number of free protons inside the viral core and

$$\alpha(P_e, P_v) = \frac{k_e^{-1} + k_v^{-1}}{k_e \left(\frac{P_e}{N_A V_e} + \frac{k_v^{-1} P_v}{k_e^{-1} N_A V_v} \right)}, \quad (25)$$

We extracted the buffer capacity of a virus and accounted for the viral genome, the internal viral proteins and unspecific buffers that can be reached through the M2 channels [20]. Most abundant internal proteins are the M1 (3,000 copies per virus) and the nucleoproteins (NP, 330 copies per virus) [18] (Figure 1-A). Proton binding sites of viral proteins are the ionogenic groups in their amino acid side chains [31], and the main ionogenic buffers in the endosome pH range are the aspartic acid (Asp, pKa=3.9), the glutamic acid (Glu, pKa=4.32) and the histidine (His, pKa=6.04) [31]. Closely related binding sites can have strong influence on each other due to electrostatic interactions.

In addition, the 3-dimensional protein folding can hinder the accessibility of some residues to the solvent and protons. Consequently, calculations based on the three-dimensional structure of the protein are necessary to determine accurately its buffering capacity with respect to pH. Using the spatial organization (crystal structure) of NP proteins [24], we computed the pKa values of all titratable residues in the proteins with electrostatic energy calculations using the software Karlsberg+ [12]. We then determined the mean number of protonated residues $n_P^{NP}(pH)$ of NP proteins (see Material and Methods) and we found that $n_P^{NP}(pH)$ increases almost linearly with pH:

$$n_P^{NP}(pH) \approx n_P^{NP}(pH = 7) + 9(7 - pH), \quad (26)$$

indicating that the buffering capacity of NPs is approximatively constant between pH 7 and 5 (equation 11)

$$\beta_v^{NP} \approx 9 \frac{330}{N_A V_v} = \frac{3000}{N_A V_v} \quad (27)$$

where $V_v = \frac{4}{3}\pi r_v^3$ is the volume of the viral internal lumen, for a spherical viral particle with radius $r_v = 60$ nm [19]. The structure of the matrix M1 protein is unknown and consequently, we use the cumulative contributions of Asp, Glu and His residues to estimate the number of M1 proton binding sites.

We thus estimate the fraction $P_i(pH)$ of occupied residues for a fixed pH using the equilibrium constant pKa_i for any residue i (Asp, Glu or His) to be

$$P_i(pH) = (10^{pH-pKa_i} + 1)^{-1}. \quad (28)$$

The mean number $n_P^{M1}(pH)$ of protonated site is then given by

$$n_P^{M1}(pH) = n_{Asp}^{M1} (10^{pH-3.9} + 1)^{-1} + n_{Glu}^{M1} (10^{pH-4.32} + 1)^{-1} + n_{His}^{M1} (10^{pH-6.04} + 1)^{-1}. \quad (29)$$

where the number of residue for each group is $n_{Asp}^{M1} = 12$, $n_{Glu}^{M1} = 12$ and $n_{His}^{M1} = 5$. Using equation 29, we plotted $n_P^{M1}(pH)$ as function of the pH and observed that $n_P^{M1}(pH)$ is almost a linear function

$$n_P^{M1}(pH) \approx n_P^{NP}(pH = 7) + 3.5(7 - pH), \quad (30)$$

and obtain that

$$\beta_v^{M1} \approx 3.5 \frac{3000}{N_A V_v} = \frac{10500}{N_A V_v}. \quad (31)$$

Additionally to internal M1s and NP proteins, protons entering the viral core through M2 channels can also bind to viral nucleic acids and in particular to basic groups in the guanine, adenine and cytosine nucleotides [31]. In particular, the buffering capacity β_v^{RNA} of oligonucleotides in solution, for a concentration $c_{monomers}$ of monomers, has been estimated to be $\beta_v^{RNA} \approx 0.1 c_{monomers}$ in the pH range 5-7 (Figure 3-D in [31]). Consequently the buffering capacity β_v^{RNA} of the ≈ 12000 viral nucleotides [10] is approximately equal to

$$\beta_v^{RNA} \approx 0.1 \frac{12000}{N_A V_v} = \frac{1200}{N_A V_v}. \quad (32)$$

Finally, the viral core lumen should also contain other unspecific buffers such as cytoplasmic buffers enclosed during the viral assembly, leading to an unspecific buffering capacity $\beta_v^0(pH)$ inside the viral lumen that has to be added to the buffering capacities β_v^{NP} and β_v^{M1} of internal proteins. Due to possible ionic exchange between viral and endosomal lumens, we approximate $\beta_v^0(pH)$ with the endosomal buffering capacity β_e^0 , which is independent of the pH and has been estimated to be [32]

$$\beta_e^0 \approx 40mM/pH. \quad (33)$$

In summary, the proton buffering capacity inside viral cores is equal to

$$\beta_i = \beta_v^0 + \beta_v^{M1} + \beta_v^{NP} + \beta_v^{RNA}, \quad (34)$$

and similarly to the flux equation 19, the number of free protons $P_v(t)$ contained in viral core at time t , which determines the influx of protons through M2 channels (equation 24), follows the kinetics equation

$$\frac{dP_v(t)}{dt} = \frac{\log(10)}{N_A V_v (\beta_v^0 + \beta_v^{M1} + \beta_v^{NP} + \beta_v^{RNA})} P_v(t) j_{M2}(P_e(t), P_v(t)). \quad (35)$$

By solving numerically equation 35, we estimate that $\approx 60,000$ protons enter the viral core during endosomal maturation. Using endosomal acidification kinetics equation 19, we estimate that more than 20,000,000 protons bind to endosomal buffers during endosome acidification. Thus, the buffering capacity of a single virus should not influence the endosomal acidification. However the number of protons that bind to endosomal buffers drastically decreases with the endosomal size (e.g. $\approx 175,000$ for $r_e = 100$ nm instead of $r_e = 500$ nm). In addition viral particles may accumulate during the endosomal journey [22]. Thus, for multiplicity of infection (MOI) and viral accumulation in endosomes, the viral buffering capacity may significantly affect the acidification kinetics of small and intermediate size endosomes.

4 Markov jump model of HA conformational change

Although the number of protons entering in the endosome is quite huge, as discussed in the previous section, the actual number of free protons defining endosomal pH is low (~ 300 at pH 6 in an endosome with a radius of 500 nm). In addition, there are few proton binding sites on a single HA that trigger its conformational change [8], which is the event we shall monitor. This change of scale between many entering protons and the few free protons and HA binding sites requires a different description than the previous continuous model. To compute the mean time for HA conformation to change as the pH drop, we shall first extract the forward and backward proton binding rates. For that purpose, we convert the HA conformational change kinetics, obtained from experimental data at various pH [16] into rate constants.

At temperature $T = 300K$, when the pH decreases from 7 to 4, the number of bound protons bound to HA1 increases approximatively from 123 to 132 (Figure 3 in [8]), suggesting that the number of available number of binding site is $n_s = 9$ at acidic pH. The influenza virus carries $n_{HA} \approx 400$ HA trimers [11] (Figure 2-A) and thus there are exactly $n_{HA}n_s$ sites that can competitively bind protons. The goal of this section is to compute the mean time that a threshold n_T of bound protons to HA1 is reached, which is a model of fusogenic state, where the protein can engage into the generation of a fusion pore with the endosomal membrane.

4.1 Modeling HA conformational change

To analyse the conformational changes of a single HA trimer, we follow the occupied sites $X(t, c)$ at time t , for a fix proton concentration c . During time t and $t + \Delta t$, the number of specific bound sites can either increase with a probability $r(X, c)\Delta t$, when a proton arrives to a free site or decreases with

probability $l(X, c)\Delta t$ when a proton unbinds or remains unchanged with probability $1 - l(X, c)\Delta t - r(X, c)\Delta t$ (Figure 2-A).

We estimate hereafter the rates $l(X, c)$ and $r(X, c)$ and the critical threshold n_T . The forward rate depends on the proton concentration c and the number of free sites $n_s - X$ of the HA trimer, thus

$$r(X, c) = Kc(n_s - X), \quad (36)$$

where K is the forward binding rate of a proton to a binding site.

To determine the proton unbinding rate $l(X, c)$, we use the values available for the HA1 protonation [8]. We approximate the number of bound protons $\tilde{X}_0(c)$ with respect to the proton concentration c by a linear function (Figure 3 [8])

$$\tilde{X}_0(c) = \tilde{X}_0(10^{-7} \text{ mol.L}^{-1}) + X_0(c) = \tilde{X}_0(10^{-7} \text{ mol.L}^{-1}) + \left(\frac{7}{3} + \frac{\log(c)}{3 \log 10}\right) n_s, \quad (37)$$

where $\tilde{X}_0(10^{-7} \text{ mol.L}^{-1})$ is the mean number of bound protons at pH=7 and

$$X_0(c) = \left(\frac{7}{3} + \frac{\log(c)}{3 \log 10}\right) n_s \quad (38)$$

is the mean number of HA1 sites that are additionally protonated for a proton concentration $c > 10^{-7} \text{ mol. L}^{-1}$. Because the unbinding rate does not depend on the proton concentration $l(X, c) = l(X)$ and we obtain for the equilibrium ratio $\frac{l(X, c)}{r(X, c)} = \frac{l(X)}{Kc(n_s - X)}$. Using at equilibrium the concentration $c(X) = 10^{\frac{3X}{n_s} - 7}$ for which $X_0(c(X)) = X$, the mass-action law leads to $\frac{l(X_0(c), c)}{r(X_0(c), c)} = 1$ or equivalently $\frac{l(X)}{Kc(X)(n_s - X)} = 1$. Finally, we get

$$l(X) = K(n_s - X)10^{\frac{3X}{n_s} - 7}. \quad (39)$$

In summary, the binding and unbinding rates r and l are given by

$$r(X, c) = Kc(n_s - X), \text{ and } l(X, c) = l(X) = K(n_s - X)10^{\frac{3X}{n_s} - 7}. \quad (40)$$

4.2 Rate of HA conformational change

To compute the mean time that exactly n_T protons are bound to a single HA we use a Markov jump process description. The Master equation is derived by evaluating during time t and $t + \Delta t$, the variation in the number of bound sites $X(t, c)$ among the $n_s = 9$ HA1 proton binding sites. The scaled variable is

$$x(t, c) = \epsilon X(t, c), \quad (41)$$

where $\epsilon = 1/n_s$ and using the difference $\Delta x = x(t + \Delta t, c) - x(t, c)$, the transition probabilities are

$$\begin{aligned} \text{Prob}\{\Delta x = \epsilon | x(t, c) = x\} &= r(x, c) \Delta t, \\ \text{Prob}\{\Delta x = -\epsilon | x(t, c) = x\} &= l(x, c) \Delta t, \\ \text{Prob}\{\Delta x = 0 | x(t, c) = x\} &= (1 - r(x, c) - l(x, c)) \Delta t. \end{aligned}$$

At a fixed proton concentration, the probability $p(y, t | x, c)$ that the number of protonated sites is equal to y at time t , that is $x(t, c) = y$, when there are initially x bound sites ($x(t = 0, c) = x$), is solution of the backward-Kolmogorov equation [21, 13, 14, 27, 17]

$$\begin{aligned} p(y, t | x, c) &= p(y, t - \Delta t | x + \epsilon, c) r(x, c) \Delta t + p(y, t - \Delta t | x - \epsilon, c) l(x, c) \Delta t \\ &\quad + p(y, t - \Delta t | x, c) (1 - r(x, c) \Delta t - l(x, c) \Delta t), \end{aligned} \quad (42)$$

which has the classical Kramers-Moyal expansion [26]

$$\begin{aligned} \frac{\partial p}{\partial t}(y, t | x, c) &= L_x p = r(x, c) \sum_{n=1}^{\infty} \frac{\epsilon^n}{n!} (\partial_x)^n p(y, t | x, c) \\ &\quad + l(x, c) \sum_{n=1}^{\infty} \frac{(-\epsilon)^n}{n!} (\partial_x)^n p(y, t | x, c). \end{aligned} \quad (43)$$

The mean first time $\tau(x, c)$ that the process $X(t, c)$ reaches the threshold $x_T = n_T/n_s$ models the HA1 subunit filled with n_s protons. It is precisely the mean of the first passage time for the bound protons $x(t, c)$ to reach the level x_T . The mean first passage time $\tau(x, c) = E[\tau | x(t = 0, c) = x]$, satisfies [27]:

$$L_x \tau(x, c) = -1 \text{ for } x \text{ in } [0, x_T], \quad (44)$$

with the boundary conditions

$$\tau(x, c) = 0 \text{ for } x = x_T \text{ and } \frac{\partial \tau(x, c)}{\partial x} = 0 \text{ for } x = 0. \quad (45)$$

For $\epsilon \ll 1$, a Wentzel-Kramers-Brillouin (WKB) [34, 15, 3] asymptotic expansion of the solution $\tau(x, c) \approx \tau(c)$ is known [14, 21, 13, 27, 17] and can be written as

$$\tau(c) \approx \frac{1}{r(x_0(c), c)} \sqrt{\frac{2\pi}{\epsilon \frac{d}{dx} \left(\frac{l}{r} \right) (x_0(c), c)}} \phi(x_T, c), \quad (46)$$

where $x_0(c)$ is the mean number of HA1 sites that are additionally protonated for a concentration $c > 10^{-7} \text{ mol.L}^{-1}$, and the dependency of x_0 with respect to the concentration c in the range $0 < x_0(c) = \epsilon X_0(c) < x_T$ has been obtained by a fitting procedure (see equation 38)

$$x_0(c) = \frac{7}{3} + \frac{\log(c)}{3 \log(10)}. \quad (47)$$

Finally, by definition,

$$\phi(x, c) = \frac{\exp\left(-\frac{1}{\epsilon} \int_{x_0(c)}^x \log\left(\frac{l(s, c)}{r(s, c)}\right) ds\right)}{\sqrt{\frac{l(x, c)}{r(x, c)}}} \left(\frac{l(x, c)}{r(x, c)} - 1\right). \quad (48)$$

Now replacing the transition rates $r(x, c)$ and $l(x)$ by their expressions 40 in equation 48 allows us to compute the mean first passage time to the threshold. Indeed,

$$\begin{aligned} \int_{x_0(c)}^{x_T} \log\left(\frac{l(s, c)}{r(s, c)}\right) ds &= \int_{x_0(c)}^{x_T} (\log(10^{3s-7}) - \log(c)) ds \\ &= \int_{x_0(c)}^{x_T} (3 \log(10)s - (7 \log(10) + \log(c))) ds, \end{aligned}$$

that is

$$\int_{x_0(c)}^{x_T} \log\left(\frac{l(s, c)}{r(s, c)}\right) ds = \int_{x_0(c)}^{x_T} (3 \log(10)s - \log(10^7 c)) ds = F(x_T) - F(x_0(c)), \quad (49)$$

where

$$F(x) = \frac{3}{2} \log(10)x^2 - \log(10^7 c)x. \quad (50)$$

leading to

$$\phi(x_T, c) = \exp\left(-\frac{1}{\epsilon} (F(x_T) - F(x_0(c)))\right) \frac{\frac{10^{3x_T-7}}{c} - 1}{\sqrt{\frac{10^{3x_T-7}}{c}}}, \quad (51)$$

that is,

$$\phi(x_T, c) = \exp\left(-\frac{1}{\epsilon} (F(x_T) - F(x_0(c)))\right) \left(\frac{10^{3x_T/2-7/2}}{\sqrt{c}} - \sqrt{c}10^{7/2-3x_T/2}\right). \quad (52)$$

Using the expressions for the binding and unbinding rates 40, we get

$$\frac{d}{dx} \left(\frac{l}{r}\right)(x_0(c), c) = \frac{d}{dx} \left(\frac{10^{3x-7}}{c}\right)(x_0(c), c) = \frac{3 \log(10)}{c} 10^{3x_0(c)-7}, \quad (53)$$

which reduces to with formula 47 to

$$\frac{d}{dx} \left(\frac{l}{r}\right)(x_0(c), c) = 3 \log(10). \quad (54)$$

Finally, with eqs 47-52 and 54, we obtain for the mean conformational change time

$$\tau(c) = \frac{\epsilon}{-Kc \left(\frac{4}{3} + \frac{\log(c)}{3 \log(10)} \right)} \frac{\sqrt{\frac{2\pi}{\epsilon 3 \log(10)}} \exp \left(\frac{1}{\epsilon} \left(F(x_T) - F \left(7/3 + \frac{\log(c)}{3 \log(10)} \right) \right) \right)}{\frac{10^{3x_T/2-7/2}}{\sqrt{c}} - \sqrt{c} 10^{7/2-3x_T/2}}. \quad (55)$$

Using that $\epsilon = 1/n_s$ and $x_T = n_T/n_s$, we finally get the new expression for the conformational change time:

$$\tau(c) = \frac{\sqrt{6\pi} \exp \left(n_s \left(F(n_T/n_s) - F \left(7/3 + \frac{\log(c)}{3 \log(10)} \right) \right) \right)}{K \sqrt{cn_s \log(10)} \left(4 + \frac{\log(c)}{\log(10)} \right) \left(c 10^{7/2-3n_T/(2n_s)} - 10^{3n_T/(2n_s)-7/2} \right)}, \quad (56)$$

where F is defined in 50.

Equation 56 links the affinities between the ligand (concentration c) and the binding sites of a trimer to the conformational change mean time $\tau(c)$ of the trimer. Interestingly, the reciprocal $\frac{1}{\tau(c)}$ has been measured for various pH values [16]: $(\tau(pH = 4.9))^{-1} = 5.78s^{-1}$, $(\tau(pH = 5.1))^{-1} = 0.12s^{-1}$, ..., $(\tau(pH = 5.6))^{-1} = 0.017s^{-1}$. Using formula 56 and a least square optimization procedure, we have approximated the data (Figure 2-B) and obtain that the critical threshold is

$$n_T \approx 6 \quad (57)$$

and the forward rate

$$K \approx 7.5 \cdot 10^3 L.mol^{-1}s^{-1}, \quad (58)$$

These two estimations can also be seen as predictions of the present model. We plotted in Figure 2-B the theoretical rate change for HA-conformational $\frac{1}{\tau(c)}$ with respect to the proton concentration c and compared it with the experimental values of [16]. We found a very good agreement (Figure 2-B), validating our jump-Markov model where the cumulative binding of few protons to an activating threshold n_T leads to HA conformational change.

4.3 A high potential barrier of HA binding sites ensures HA stability at neutral pH

We have seen in section that during endosomal acidification, a huge number of protons enter the endosome (more than $20 \cdot 10^6$ and bind mostly to endosome buffers, leaving very few free protons (around 300 at pH 6)). To test whether HAs buffer entering protons or interact with the remaining few free protons,

we estimate the potential barrier generated at each HA binding site. For this purpose, we compare the reciprocal of the forward rate constant K (equation 58), which is the mean time for a proton to bind a HA protein, with the free Brownian diffusion time scale. For a fixed proton concentration at a value c , the proton binding time is $\tau_{bind} = \frac{1}{Kc}$, while the mean time for a proton to diffuse to the same binding site is [33,30,29,28]

$$\tau_{diff} \approx \frac{V}{4\pi D_p \eta} n(c) \quad (59)$$

. The number of endosomal protons at concentration c is $n(c) = N_A c V$, while η is the interacting radius between a proton and a binding site and D_p the diffusion constant of a free proton ($D_p \approx 100 \mu m^2 s^{-1}$ measured in the cytoplasm [1]). For $\eta = 1 nm$, we find a small ratio

$$\frac{\tau_{diff}}{\tau_{bind}} = \frac{K}{4\pi D_p \eta N_A} \approx 10^{-4}. \quad (60)$$

confirming that the mean time for a proton to bind HA is dominated by a very high activation energy barrier at the HA binding sites, preventing rapid proton binding. Consequently, the buffering capacity of HAs can be neglected compared to the high capacity of other endosomal buffers. In addition, our model predicts that high HA1 potential barrier guarantees that the conformational change is only triggered after a cumulative binding of $n_T = 6$ protons, ensuring a high stability of the protein at pH above 6, as previously characterized in Table 2 of [16] and confirmed in Figure S1.

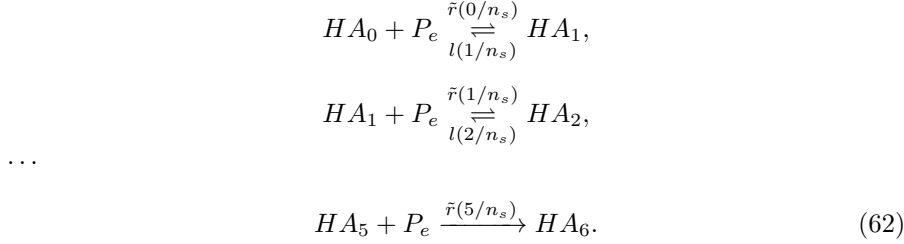
In summary, we found that the threshold for HA1 conformational change occurs when there are $n_T = 6$ bound proton in a total of $n_s = 9$ binding sites. The binding is characterized by a very high potential barrier. Thus, when protons enter an endosome, they will first be captured by endosomal buffers. The remaining pool of free protons can bind to HA1 sites when they succeed passing the high potential barrier to ultimately trigger HA conformational change.

5 A complete model of virus-endosome fusion

Combining the kinetics model of endosome acidification with the Markov jump model of HA conformational change, we now propose a kinetics model of HAs conformational change inside an endosome. We account for the $n_T = 6$ protons activating a HA1 trigger leading to HA conformational change. We shall estimate the numbers $HA_0(t), HA_1(t) \dots HA_6(t)$ of viral HAs that have $0, 1 \dots 6$ bound protons at time t , and compute the number of fusogenic (active) $HA_6(t)$, responsible for membrane fusion. From relation 36, the forward rate of a proton to a free HA1 binding site is

$$\tilde{r}(X) = r(X, P_e(t)) / P_e(t) = \frac{K n_s (n_s - X)}{N_A V_e}. \quad (61)$$

and the backward rate $l(X)$ is given by relation 40, thus the chemical equations for protons P_e and HA proteins are summarized by



where the rate constant depends on each stage as given by relation 61. The stage HA_6 is irreversible and the kinetic rate equations are

$$\begin{aligned}
 \frac{dHA_0(t)}{dt} &= -\tilde{r}\left(\frac{0}{n_s}\right) P_e(t) HA_0(t) + l\left(\frac{1}{n_s}\right) HA_1(t), \\
 \frac{dHA_1(t)}{dt} &= \left(\tilde{r}\left(\frac{0}{n_s}\right) HA_0(t) - \tilde{r}\left(\frac{1}{n_s}\right) HA_1(t)\right) P_e(t) + l\left(\frac{2}{n_s}\right) HA_2(t) - l\left(\frac{1}{n_s}\right) HA_1(t), \\
 &\dots
 \end{aligned} \tag{63}$$

$$\frac{dHA_6(t)}{dt} = \tilde{r}\left(\frac{5}{n_s}\right) HA_5(t) P_e(t). \tag{64}$$

Given the proton entry rate (equation 19), these equations can be solved numerically.

5.1 Modeling the onset of fusion between virus and endosome membranes

The onset of membrane fusion is triggered by the conformational change of multiple adjacent trimer in the contact zone between virus and endosome membranes [4, 11]. However, the number of fusogenic HAs involved in formation and fusion pore enlargement is still an open question.

We model the contact zone between the virus and endosome membranes by 120 HAs among the 400 covering the virus [11](Figure3-A). Then, using a numerical solution of equation 64, we chose randomly each new fusogenic HA and defines the onset of virus endosome fusion by the stochastic activation of Na adjacent HAs in the contact zone (Figure 3-A). Using 1,000 Monte-Carlo simulations, we estimated the mean and confidence interval at 95% of the fusion onset time for different Na .

We found that for $Na = 1$ or 2 , most viruses fuse in EE, whereas for $Na = 3$ or 4 viruses fuse in ME. Finally, for $Na = 5$ or 6 , viruses mostly fuse in LE (Figure 3-B,C). The common prediction is that $Na = 3 - 4$ [4, 11] indicating that viruses shall fuse in ME.

5.2 Probing the intracellular localization of fusion with live cell imaging

To determine the localization of virus fusion, we used the fluorescent endosomal markers Rab5 (EE) and Rab7 (LE) in combination with an intracellular fusion assay to detect virus-endosome fusion so that the localization to a specific compartment can be assigned. Single virus spots were analyzed, where fusion was indicated by a pronounced increase of spot signal (Figure S2). To determine the cellular localization of virus fusion, we analyse infected Rab5- and Rab7-expressing cells with R18-labeled viruses (Figure 3-D). We classified single endosomes based on the presence of the two Rab proteins into three classes (Figure S3). Early endosomes (EE) do not show Rab7 association, such as late endosomes (LE) do not possess Rab5 signal. If endosomes possess both signals, they were counted as maturing endosomes (ME). We observe a gradual increase of Rab7 along with a decrease of Rab5 (Figure 3-D). After 5 min, we rarely observe fusion events in Rab5-only endosomes. The majority of fusion events (61%) are detected in maturing endosomes between 10-20 min post infection (Figure 3-E). At later time points, the localization of fusion events shifted towards late endosomes. However, de-quenching kinetics show that fusion mostly occurs between 10-20 min (Figure S2).

We thus conclude that virus fusion was essentially associated with maturing endosomes indicating that $Na = 3$ or 4 adjacent fusogenic HA are needed to mediate fusion .

6 Discussion

Influenza viruses are internalized into endosomes via receptor-mediated endocytosis. During their transport along microtubules, the endosomes accumulate protons, which eventually enable virus-endosome fusion mediated by the influenza HA, resulting in release of the viral genome in the cell cytoplasm. Hence, the duration of endosomal transport as well as the localization of fusion critically depend on endosomal acidification and HA conformational change at low pH. Here we presented a new model to investigate the role of key parameters that shape the endosomal residence time of influenza viruses.

By associating a kinetics model of endosomal acidification with a Markov-jump process model of HA conformational change, we estimated the number of fusogenic HAs as function of time inside endosomes, and we modeled the onset of fusion with the stochastic activation of Na adjacent HAs. Using the model, we predict the high HA stability at neutral pH due to the high activation barrier of protons binding sites. In association with $Na \geq 3$, this ensures that fusion occurs in ME, preventing a premature fusion in EE. As endosomal maturation is associated with retrograde transport of endosomes along MTs, this should increase the nuclear targeting of viral genome and pathogenicity of the virus.

Acknowledgements This research was supported by an Marie Curie grant (D.H.), by the Deutsche Forschungsgemeinschaft (HE 3763/15-1) (A.H.) and the Bundesministerium für Bildung und Forschung (eBio: ViroSign) (CS and AH). T.L. is funded by a Bourse Roux from Institut Pasteur.

References

1. al Baldawi, N.F., Abercrombie, R.F.: Cytoplasmic hydrogen ion diffusion coefficient. *Biophys J* **61**(6), 1470–9 (1992). DOI 10.1016/S0006-3495(92)81953-7
2. Bayer, N., Schober, D., Prchla, E., Murphy, R.F., Blaas, D., Fuchs, R.: Effect of bafilomycin A1 and nocodazole on endocytic transport in hela cells: implications for viral uncoating and infection. *J Virol* **72**(12), 9645–55 (1998)
3. Brillouin, L.: La mécanique ondulatoire de schrodinger: une méthode générale de résolution par approximations successives. *Comptes Rendus de l'Academie des Sciences* (183)
4. Danieli, T., Pelletier, S.L., Henis, Y.I., White, J.M.: Membrane fusion mediated by the influenza virus hemagglutinin requires the concerted action of at least three hemagglutinin trimers. *J Cell Biol* **133**(3), 559–69 (1996)
5. Fuchs, R., Schmid, S., Mellman, I.: A possible role for Na⁺/K⁺-ATPase in regulating ATP-dependent endosome acidification. *Proc Natl Acad Sci U S A* **86**(2), 539–43 (1989)
6. Grabe, M., Oster, G.: Regulation of organelle acidity. *J Gen Physiol* **117**(4), 329–44 (2001)
7. Grabe, M., Wang, H., Oster, G.: The mechanochemistry of v-ATPase proton pumps. *Biophys J* **78**(6), 2798–813 (2000). DOI 10.1016/S0006-3495(00)76823-8
8. Huang, Q., Opitz, R., Knapp, E.W., Herrmann, A.: Protonation and stability of the globular domain of influenza virus hemagglutinin. *Biophys J* **82**(2), 1050–8 (2002). DOI 10.1016/S0006-3495(02)75464-7
9. Huang, Q., Sivaramakrishna, R.P., Ludwig, K., Korte, T., Böttcher, C., Herrmann, A.: Early steps of the conformational change of influenza virus hemagglutinin to a fusion active state: stability and energetics of the hemagglutinin. *Biochim Biophys Acta* **1614**(1), 3–13 (2003)
10. Hutchinson, E.C., von Kirchbach, J.C., Gog, J.R., Digard, P.: Genome packaging in influenza A virus. *The Journal of general virology* **91**(Pt 2), 313–328 (2010)
11. Ivanovic, T., Choi, J.L., Whelan, S.P., van Oijen, A.M., Harrison, S.C.: Influenza-virus membrane fusion by cooperative fold-back of stochastically induced hemagglutinin intermediates. *Elife* **2**, e00333 (2013). DOI 10.7554/eLife.00333
12. Kieseritzky, G., Knapp, E.W.: Optimizing pKa computation in proteins with pH adapted conformations. *Proteins: Structure, Function, and Bioinformatics* **71**(3), 1335–1348 (2008). DOI 10.1002/prot.21820. URL <http://dx.doi.org/10.1002/prot.21820>
13. Knessl, C., Mangel, M., Matkowsky, B., Schuss, Z., Tier, C.: Solution of Kramers-Moyal equations for problems in chemical physics. *Journal of Chemical Physics* **81**(3), 1285–1293 (1984)
14. Knessl, C., Matkowsky, B., Schuss, Z., Tier, C.: An asymptotic theory of large deviations for Markov jump-processes. *Siam Journal On Applied Mathematics* **45**(6), 1006–1028 (1985)
15. Kramers, H.A.: Wellenmechanik und halbzahlige Quantisierung. *Zeitschrift für Physik* **39** (1926)
16. Krumbiegel, M., Herrmann, A., Blumenthal, R.: Kinetics of the low pH-induced conformational changes and fusogenic activity of influenza hemagglutinin. *Biophys J* **67**(6), 2355–60 (1994). DOI 10.1016/S0006-3495(94)80721-0
17. Lagache, T., Danos, O., Holcman, D.: Modeling the step of endosomal escape during cell infection by a nonenveloped virus. *Biophys J* **102**(5), 980–9 (2012). DOI 10.1016/j.bpj.2011.12.037
18. Lamb, R., Krug, R.: Orthomyxoviridae: The viruses and replication. In: D. Knipe, P. Howley, D. Griffin (eds.) *Fields Virology*, 4th edn. Lippincott Williams and Wilkins (1996)

19. Lamb, R.A., Choppin, P.W.: The gene structure and replication of influenza virus. *Annu Rev Biochem* **52**, 467–506 (1983). DOI 10.1146/annurev.bi.52.070183.002343
20. Leiding, T., Wang, J., Martinsson, J., DeGrado, W.F., Arsköld, S.P.: Proton and cation transport activity of the m2 proton channel from influenza a virus. *Proc Natl Acad Sci U S A* **107**(35), 15,409–14 (2010). DOI 10.1073/pnas.1009997107
21. Matkowsky, B., Schuss, Z., Knessl, C., Tier, C., Mangel, M.: Asymptotic solution of the kramers-moyal equation and first-passage times for markov jump processes. *Phys. Rev. A* **29**, 3359–3369 (1984)
22. Matlin, K.S., Reggio, H., Helenius, A., Simons, K.: Pathway of vesicular stomatitis virus entry leading to infection. *J Mol Biol* **156**(3), 609–31 (1982)
23. Mercer, J., Schelhaas, M., Helenius, A.: Virus entry by endocytosis. *Annu Rev Biochem* **79**, 803–33 (2010). DOI 10.1146/annurev-biochem-060208-104626
24. Ng, A.K.L., Zhang, H., Tan, K., Li, Z., Liu, J.h., Chan, P.K.S., Li, S.M., Chan, W.Y., Au, S.W.N., Joachimiak, A., Walz, T., Wang, J.H., Shaw, P.C.: Structure of the influenza virus a h5n1 nucleoprotein: implications for rna binding, oligomerization, and vaccine design. *FASEB J* **22**(10), 3638–47 (2008). DOI 10.1096/fj.08-112110
25. Rink, J., Ghigo, E., Kalaidzidis, Y., Zerial, M.: Rab conversion as a mechanism of progression from early to late endosomes. *Cell* **122**(5), 735–49 (2005). DOI 10.1016/j.cell.2005.06.043
26. Risken, H.: *The Fokker-Planck Equation: Methods Of Solution And Applications*. Springer (1996)
27. Schuss, Z.: *Theory and Applications of Stochastic Processes*. Springer (2010)
28. Schuss, Z., Holcman, D.: *Stochastic Narrow Escape in Molecular and Cellular Biology: Analysis and Applications*. Springer (2015)
29. Schuss, Z., Singer, A., Holcman, D.: The narrow escape problem for diffusion in cellular microdomains. *Proc Natl Acad Sci U S A* **104**(41), 16,098–103 (2007). DOI 10.1073/pnas.0706599104
30. Singer, A., Schuss, Z., Holcman, D.: Narrow escape, part iii: Non-smooth domains and riemann surfaces. *J Stat Phys* **122**(3), 491–509 (2006)
31. Stoyanov, A., Righetti, P.: Buffer properties of biopolymer solutions, as related to their behaviour in electrokinetic methodologies. *Journal of Chromatography A* **838**, 11–18 (1999)
32. Van Dyke, R.W., Belcher, J.D.: Acidification of three types of liver endocytic vesicles: similarities and differences. *Am J Physiol* **266**(1 Pt 1), C81–94 (1994)
33. Ward, M., Keller, J.: Strong localized perturbations of eigenvalue problems. *Siam Journal On Applied Mathematics* **53**(3), 770–798 (1993)
34. Wentzel, G.: Eine verallgemeinerung der quantenbedingungen fur die zwecke der wellenmechanik. *Zeitschrift fur Physik* **38** (1926)
35. Zaraket, H., Bridges, O.A., Duan, S., Baranovich, T., Yoon, S.W., Reed, M.L., Salomon, R., Webby, R.J., Webster, R.G., Russell, C.J.: Increased acid stability of the hemagglutinin protein enhances h5n1 influenza virus growth in the upper respiratory tract but is insufficient for transmission in ferrets. *J Virol* **87**(17), 9911–22 (2013). DOI 10.1128/JVI.01175-13

Figures and tables

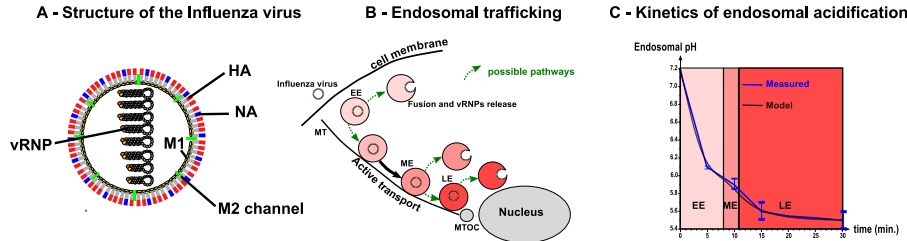


Fig. 1 Structure and endosomal trafficking of the Influenza virus
A - Structure of the Influenza virus. Influenza is an enveloped virus. Main spike proteins anchored in the envelope are the neuraminidase (NA) and the HA (HA). Protons can access the core of the virus through M2 channels. Main matrix protein is M1 protein. Viral genome of the virus is composed by eight viral ribonucleoproteins (vRNPs). **B Endosomal trafficking of the virus.** Influenza virus enters the cell via receptor-mediated endocytosis and progress rapidly towards an Early Endosome (EE). Then, maturation of EE into a Maturing Endosome (ME) and Late Endosome (LE) is associated with an acidification of the endosome lumen and a retrograde transport of the endosome along the microtubules (MTs) of the cell towards the nucleus, the destination of vRNPs for virus replication. Fusion between the virus and the endosome membrane is critically controlled by the low pH conformational change of HAs, but the kinetics of in vivo escape remains largely unknown. **C- Kinetics of endosomal pH decrease** obtained from intracellular fluorescence microscopy (red line. Mean \pm SEM) and coarse-grained modeling (equation 19, black line. Model parameters are summarized in table 1).

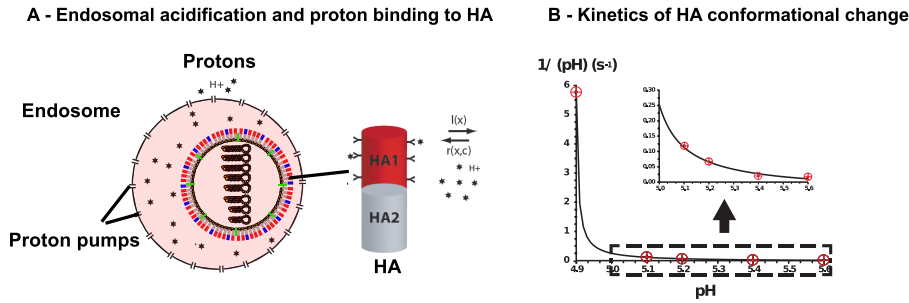


Fig. 2 Free protons in the endosome triggers HA conformational change
A - Schematic representation of the influenza virus inside an endosome. The right-hand side shows a scheme of an isolated HA trimer. Free protons in the endosome can bind to HA trimers. The protons binding rates $r(X, c)$ and $l(X)$ depend on the number of occupied sites X and on the concentration c of free protons in the endosome. When the number of bound protons reaches a given threshold, the HA trimer changes conformation into a fusogenic state. **B Rate of the HA conformational change as a function of the pH.** The theoretical curve (solid line) for the rate of HA conformational change $(\tau(c))^{-1}$ approximate well the experimental data (red circled crosses) [16]. The region inside the dashed box is magnified in the upper inset.

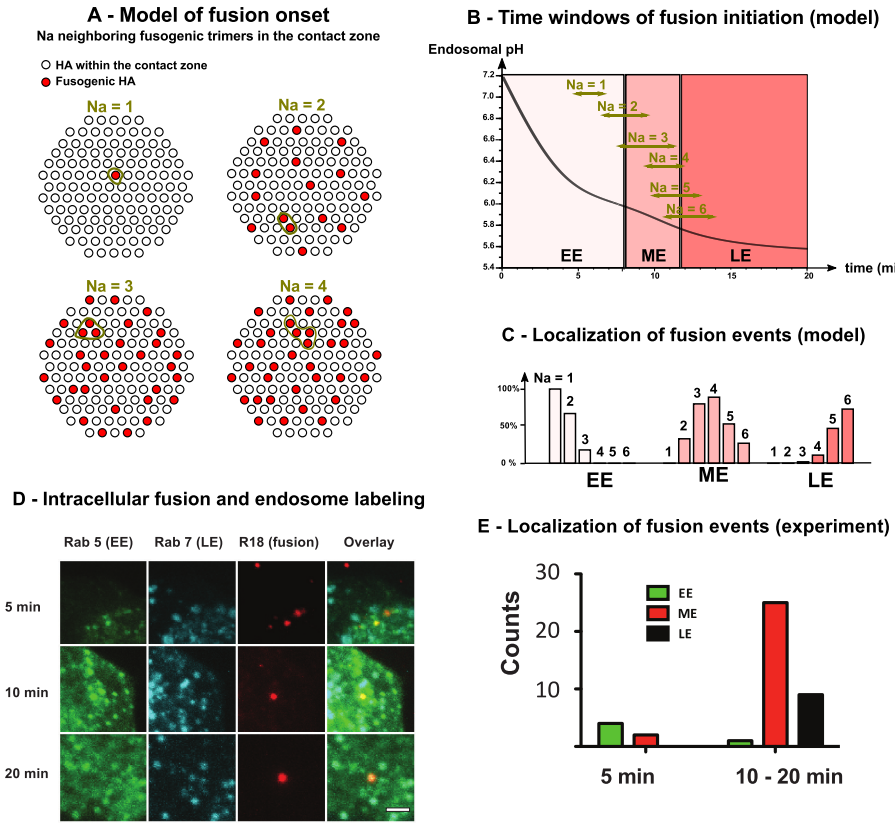


Fig. 3 Model and fluorescence experiments of the intracellular onset of virus-endosome fusion **A - Model of fusion onset.** The fusion between virus and endosome membranes is triggered by the conformational change of N_a adjacent HAs in the contact zone between virus and endosome (≈ 120 among the 400 HAs covering the virus envelope [11]). **B - Modeling the stochastic activation of HAs on virus envelope during endosomal trafficking.** Solving equation 64 we estimated the time window (95% confidence interval) of intracellular fusion for $1 \leq N_a \leq 6$. **C - Localization of fusion events as function of N_a .** Using time windows of fusion onset and endosome maturation kinetics (equation 20), we estimated the localization (EE, ME or LE) of fusion onset as function of the number N_a of adjacent fusogenic HAs needed for the fusion onset. **D - In vivo monitoring of fusion between virus and endosomes.** MDCK cells expressing Rab5-CFP and Rab7-GFP were incubated with R18-labeled influenza A viruses. Fusion was observed as a strong increase of R18 signal due to de-quenching after dilution. Scale bar = $1 \mu m$ **E - In vivo localization of fusion events.** Fusion events were counted and categorized regarding their localization in EE (Rab5), ME (Rab5 + Rab7) or LE (Rab7).

Table 1 Parameters of the endosome acidification model

Parameters	Description	Value
r_e	Radius of the endosome	$r_e = 500\text{nm}$ [25]
V_e	Volume of the endosome	$V_e = \frac{4}{3}\pi r_e^3 = 5.22 \cdot 10^{-16}\text{L}$
r_v	Radius of the influenza virus	$r_v = 60\text{nm}$ [19]
V_v	Volume of the viral internal lumen	$V_v = \frac{4}{3}\pi r_v^3 = 9 \cdot 10^{-19}\text{L}$
N_A	Avogadro constant	$N_A = 6.02 \cdot 10^{23}\text{mol}^{-1}$
β_e^0	Buffering capacity of the endosomal lumen	$\beta_e^0 = 40\text{mM/pH}$ [32]
β_v^0	Buffering capacity of the viral lumen	$\beta_v^0 = \beta_e^0 = 40\text{mM/pH}$ (this study)
β_v^{M1}	Buffering capacity of viral M1s	$\beta_v^{M1} \approx \frac{10500}{N_A V_v} \text{mM/pH}$ (this study)
β_v^{NP}	Buffering capacity of viral NPs	$\beta_v^{NP} \approx \frac{3000}{N_A V_v} \text{mM/pH}$ (this study)
β_v^{RNA}	Buffering capacity of viral RNA	$\beta_v^{RNA} \approx \frac{1200}{N_A V_v} \text{mM/pH}$ (figure 3-D in [31])
L^{early}	Permeability constant of early endosomes	$L^{\text{early}} \approx 3.5 \cdot 10^{-3} N_A \text{cm s}^{-1}$ (this study)
L^{late}	Permeability constant of late endosomes	$L^{\text{late}} \approx 3.5 \cdot 10^{-4} N_A \text{cm s}^{-1}$ (this study)
$\text{pH}_{\infty}^{\text{early}}$	Steady state pH of early endosomes	$\text{pH}_{\infty}^{\text{early}} = 6.0$ [2]
$\text{pH}_{\infty}^{\text{late}}$	Steady state pH of late endosomes	$\text{pH}_{\infty}^{\text{late}} = 5.5$ [2]
$t_{1/2}$	Half maturation time of endosomes	$t_{1/2} = 10\text{min.}$ (this study)
τ_c	Rab5/Rab7 mean conversion time	$\tau_c = 100\text{s}$ (figure 4-C in [25])

Table 2 Parameters of the HA's change of conformation model

Parameters	Description	Value
$r(x, c)$	Binding rate	$r(x, c) = K c n_s (1 - x)$ (this study)
$l(x)$	Unbinding rate	$l(x) = K n_s (1 - x) 10^{-(3(1-x)+4)}$ [8]
n_T	Critical threshold for the number of HA1 bound sites	$n_T = 6$ (this study)
K	Binding rate of a proton to a free HA1 binding site	$K = 7.5 \cdot 10^3 \text{L.mol}^{-1}\text{s}^{-1}$ (this study)
$n_s = 1/\epsilon$	Number of HA1 binding sites	$n_s = 9$ [8]
n_{HA}	Number of HAs	$n_{HA} = 400$ [11]